Chapter 6

Investigating anomalous thermal expansion and ferroelectrovolume effect in a Sodium Niobate based relaxor

6.1 Introduction

Thermal expansion is an important issue in solid-state chemistry, which generally correlates with its crystal structure, microstructure, defects, etc. [330]. Thermal stress may lead to device failure as a result of an undesirable mismatch in the coefficients of thermal expansion [331]. Consequently, it is crucial to synthesise materials with precisely controlled thermal expansion properties. Control of thermal expansion can be accomplished either in single-phase materials or by creating composite materials [331, 332, 333]. However, achieving anomalous thermal expansion within a single-phase material is generally preferred, as it helps to avoid issues such as poor interfacial bonding and unwanted surface chemical reactions [270, 331].

The anharmonic nature of lattice vibrations is the precursor for the thermal expansion of solids [330]. Generally, the temperature dependence of the volume of solids can

be described using the Debye-Grüneisen relationship [334, 335]. When the thermal expansion of a material differs from the theoretical value predicted by the Debye-Grüneisen equation, it is typically described as exhibiting anomalous thermal expansion. In that case, the thermal expansion could be more positive, zero, or negative. The progress in the functional materials has shown a general physical picture that anomalous thermal expansion can be correlated with physical properties, such as ferroelectricity, magnetism, charge transfer, and superconductivity [336, 337, 338, 339, 340, 341]. The anomalous thermal expansion in ferroelectrics results from two competitive factors, anharmonic phonon vibration and ferroelectric order, which contribute to positive and negative thermal expansion, respectively [330]. Therefore, the thermal expansion of ferroelectrics can be manipulated by tailoring ordering at long ranges(conventional ferroelectrics) and/or short ranges(relaxor ferroelectrics).

Anomalous thermal expansion (ATE) in ferroelectric and relaxor ferroelectric materials has attracted considerable attention due to its unique origin, which is linked to the interplay between local polarisation, structural distortions, and temperature-dependent phase transitions [131, 337, 342, 343, 344, 345]. In conventional ferroelectrics, ATE is typically associated with the coupling between lattice strain and macroscopic spontaneous polarization [346]. This coupling (known as ferroelectrostriction or ferroelectrovolume effect) induces a contraction in unit cell volume below the Curie temperature T_C [347]. In contrast to classical ferroelectrics, relaxor ferroelectrics present a more complex picture. These materials do not exhibit a sharp phase transition at T_m, instead show a diffuse dielectric maximum and strong frequency dispersion in dielectric permittivity [120, 122, 125, 129, 295, 348, 349]. This behaviour is primarily attributed to the formation of locally polarised regions, which are commonly referred to as polar nano-regions (PNRs). In typical relaxors, these PNRs form below a characteristic temperature known as the Burns temperature (T_B) [130]. The PNRs are dynamic and randomly oriented at high tem-

peratures but gradually develop static correlations as the temperature decreases. Despite the lack of long-range ferroelectric order, these correlated PNRs lead to unusual thermal expansion behaviour due to substantial strain on the lattice. Several investigations have observed ATE in relaxor materials such as $PbMg_{1/3}Nb_{2/3}O_3$ (PMN), $PbZn_{1/3}Nb_{2/3}O_3$ (PZN), $PbMg_{1/3}Ta_{2/3}O_3$ (PMT), $PbFe_{2/3}W_{1/3}O_3$ (PFW) and so on [131, 345, 350, 351]. In these systems, the extent of polar ordering and lattice strain is closely related to the magnitude of volume anomalies. Furthermore, the intensity of ATE is associated with chemical disorder and the degree of cation off-centring, both of which influence polarizability and the interactions among local dipoles.

In this work, we investigate the origin of anomalous thermal expansion in a lead-free sodium niobate-based relaxor system, namely (1-x)$NaNbO_3$–x($Ba_{0.9}Ca_{0.1}$)TiO_3 with $x = 0.60$ (hereafter referred to as NN-60BCT). Previous dielectric and Raman studies on this composition have indicated relaxor-like characteristics, where short-range polar symmetry has been observed in the long-range non-polar matrix [71]. In the present work, we have studied the evolution of long- and short-range structures of NN-60BCT using the temperature-dependent Synchrotron X-ray diffraction, Raman spectroscopy, and Pair Distribution function analysis in connection with dielectric analysis. The unit cell volume of the two cubic phases(C_{BT} and C_{NN}) obtained from Le-bail analysis of SXRD data reveals a pronounced deviation from nominal thermal expansion, suggesting the presence of ferroelectrostriction at low temperatures. To investigate the microscopic origin of this behaviour, we combined the results obtained from temperature-dependent Raman and PDF analysis in a wide temperature range ($100 \leq T \leq 500$ K). Our results demonstrate the presence of coexisting short-range polar distortions with tetragonal and rhombohedral symmetry, embedded in non-polar matrices with the same long-range symmetries. The enhanced correlations among the PNRs at low temperatures were held responsible for the observed anomalous thermal expansion (ferroelectrovolume effect).

6.2 Experimental Section

Samples with nominal composition 0.40 $NaNbO_3$–0.60 $Ba_{0.9}Ca_{0.1}TiO_3$ (NN-60BCT) were synthesized via the conventional solid-state reaction route (see experimental section from chapter 3 for more details). The Synchrotron X-ray Diffraction and PDF (Pair Distribution Function) data were collected using Beamline 28-ID-2 (X-ray Powder Diffraction, XPD) at NSLS2 (National Synchrotron Light Source), at Brookhaven National Laboratory, with a wavelength of 0.18210 Å. High-Q measurements were conducted with a maximum instrumental Q value (Q_{max}) of 18.1 $Å^{-1}$. The structural refinements of the experimental atomic PDFs were carried out using the PDFgui program [225].

Silver electrodes were fired on the top and bottom surfaces of the samples for the electrical measurements. The dielectric measurements were carried out using a Keysight LCR meter in the temperature range of 100 K - 550 K. Temperature-dependent Raman measurements were performed using a Horiba LabRAM HR spectrometer equipped with an Olympus BX41 microscope. An excitation wavelength of 514.5 nm from a Lexel Model-95 argon ion laser was used (see experimental section of chapter 5 for more details). All Raman spectra were corrected using the Bose-Einstein temperature factor. Further, Raman spectra were deconvoluted and fitted using the Lorentzian function.

6.3 Results and discussions

6.3.1 Dielectric studies

Figure 6.1 depicts the temperature-dependent real and imaginary parts of the dielectric permittivity for NN-60BCT at various frequencies. As discussed in chapter 3, the dielectric permittivity shows a diffuse and frequency-dependent maximum, typical of relaxor ferroelectrics [71]. Interestingly, unlike the real part, there are two peaks in the imaginary part of the dielectric permittivity. The first peak at T $\approx$ 150 K corresponds to the maximum

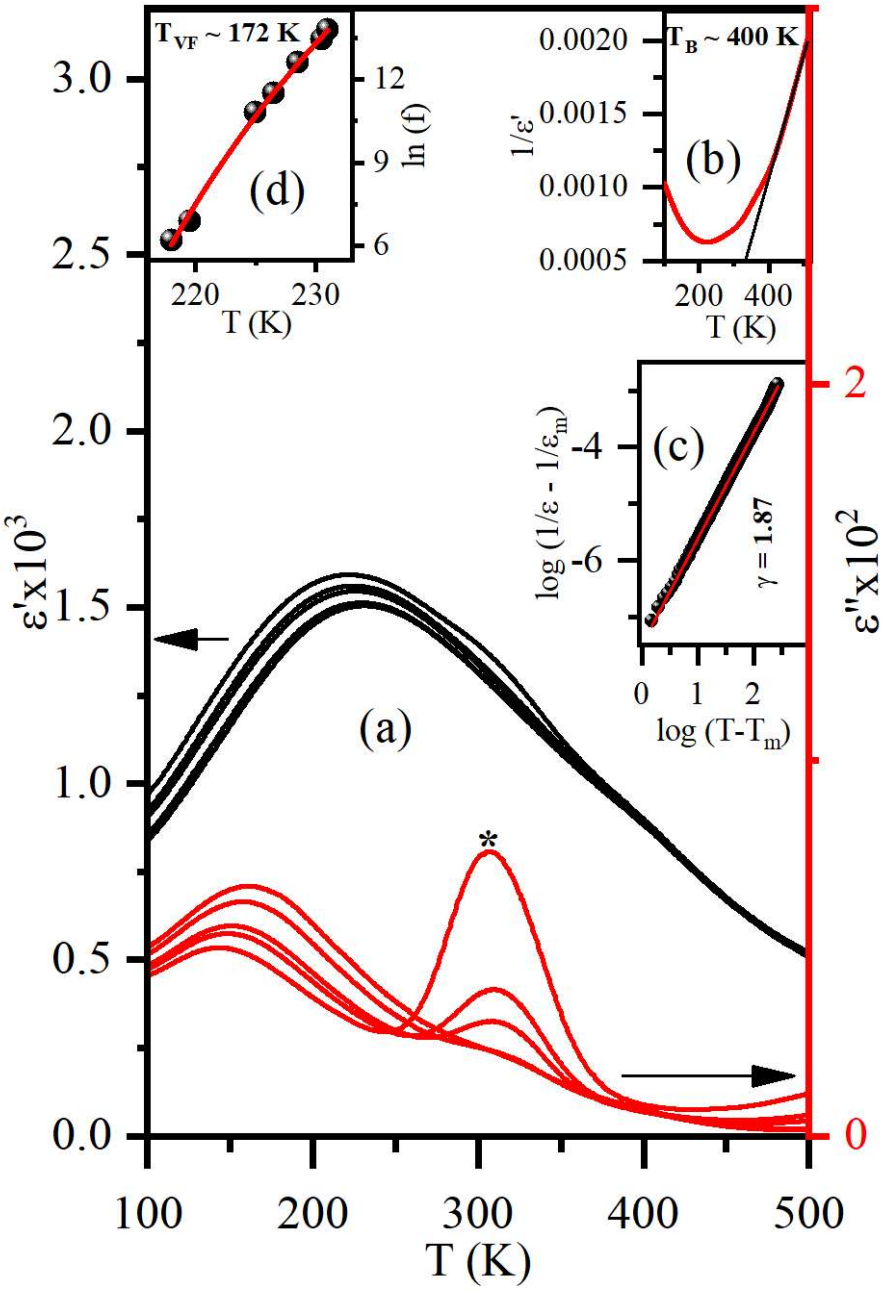

Fig. 6.1 (a) Temperature-dependent evolution of real and imaginary part of dielectric permittivity, (b) The inverse of the dielectric permittivity as a function of temperature marks the Burns Temperature,(c) linear fitting of $\log(1/\varepsilon'\text{-}1/\varepsilon'_m)$ vs. $\log(\text{T-T}_\text{m})$ at 100 KHz (d) Vogel-Fulcher fitting of the temperatures corresponding to the dielectric to estimate the freezing temperature.

of the real part of the dielectric permittivity. The second peak at T $\approx$ 300 K (prominent at low frequencies) has been attributed to the electron-hole conduction mechanism and space charge polarisation similar to what has been reported earlier for relaxors [144, 352, 353].

A characteristic feature of the dielectric response in relaxor materials is significant deviation from Curie–Weiss law above T_m (see Fig. 6.1 (b)). The temperature at which this deviation occurs is referred to as Burns temperature in the literature, and is linked with the nucleation and growth of polar nanoregions (PNRs) [128]. The Burns temperature (T_B) for NN-60BCT is $\approx$ 400 K. The modified Curie-Weiss law is used to describe the dielectric permittivity of relaxor ferroelectrics, which shows departure from the Curie-Weiss law [245]. The modified Curie-Weiss law is expressed as:

$$\frac{1}{\varepsilon'} - \frac{1}{\varepsilon_m} = \frac{(T - T_m)^\gamma}{C} \tag{6.1}$$

Here, γ and C are constants. Moreover, $\gamma = 1$ corresponds to normal ferroelectrics and $\gamma = 2$ corresponds to ideal relaxor ferroelectrics [245]. Figure 6.1 (c) presents the fitting of the dielectric permittivity data using the modified Curie-Weiss law at 100 kHz. The fitting gives a value of $\gamma = 1.87$, indicating the diffuse nature of dielectric permittivity for NN-60BCT.

Now, in order to analyze the frequency dependence of the temperatures corresponding to dielectric permittivity maximum (T_{max}), an empirical Vogel-Fulcher (VF) relationship has been used in analogy to the magnetic relaxation observed in spin-glass systems [149]. VF relationship is expressed as :

$$f = f_0 \exp\left[-\frac{E_a}{k(T_{\max} - T_{VF})}\right] \tag{6.2}$$

where T_{VF} is the static freezing temperature, E_a is the activation energy, f_o is an attempt frequency, and T_{max} is the temperature of the dielectric permittivity maximum [149]. Fig.

6.1 (d) shows Vogel-Fulcher fitting of the real part of dielectric permittivity for NN-60BCT in the frequency range of 500 Hz to 1 MHz. Vogel-Fulcher freezing temperature obtained after fitting the temperatures corresponding to the dielectric maximum gives $T_{VF} \approx 172$ K. As discussed in the previous chapter, canonical relaxors exhibit a long-range paraelectric phase with $Pm\bar{3}m$ space group stable down to the lowest temperatures. However, some relaxors experience a long-range ferroelectric phase transition at low temperature (i.e., below T_{VF}) [137, 138, 139, 140, 141, 304]. In the next section, we use diffraction methods to investigate a possible long-range structural phase transition at low temperatures (if any).

6.3.2 Synchrotron X-ray diffraction studies

To explore the structural evolution of NN-60BCT as a function of temperature, variable temperature Synchrotron X-ray diffraction (SXRD) measurements were conducted in a wide temperature range (100 K $\leq$ T $\leq$ 500 K) in heating mode. Figure 6.2 depicts the temperature-dependent evolution of a few representative main perovskite reflections, *viz.,* $\{200\}_{pc}$, $\{220\}_{pc}$, and $\{222\}_{pc}$. Here, indexing of the Bragg's reflections has been done with respect to a pseudocubic (pc) perovskite cell. As presented in Chapter 3, the main perovskite reflections of NN-60BCT seem to split into two at ambient conditions. The main perovskite reflections in the paraelectric region were fixed with the two long-range cubic phases (space group: $Pm\bar{3}m$) *viz.,* C_{BT} (associated with a larger unit cell volume) and C_{NN} (associated with a smaller unit cell volume), corresponding to Barium Titanate (BT) and Sodium Niobate (NN), respectively. Figure 6.2 clearly depicts that the splitting pattern of the main perovskite reflections remains unchanged for the studied temperature range (100 K $\leq$ T $\leq$ 500 K). Thus, it can be concluded that no long-range structural phase transition takes place within this temperature range. Therefore, a model with two cubic phases could fix the diffraction patterns of NN-60 BCT at all the measured temperatures. Following this analysis, we performed Le-bail refinements using a model with two cubic

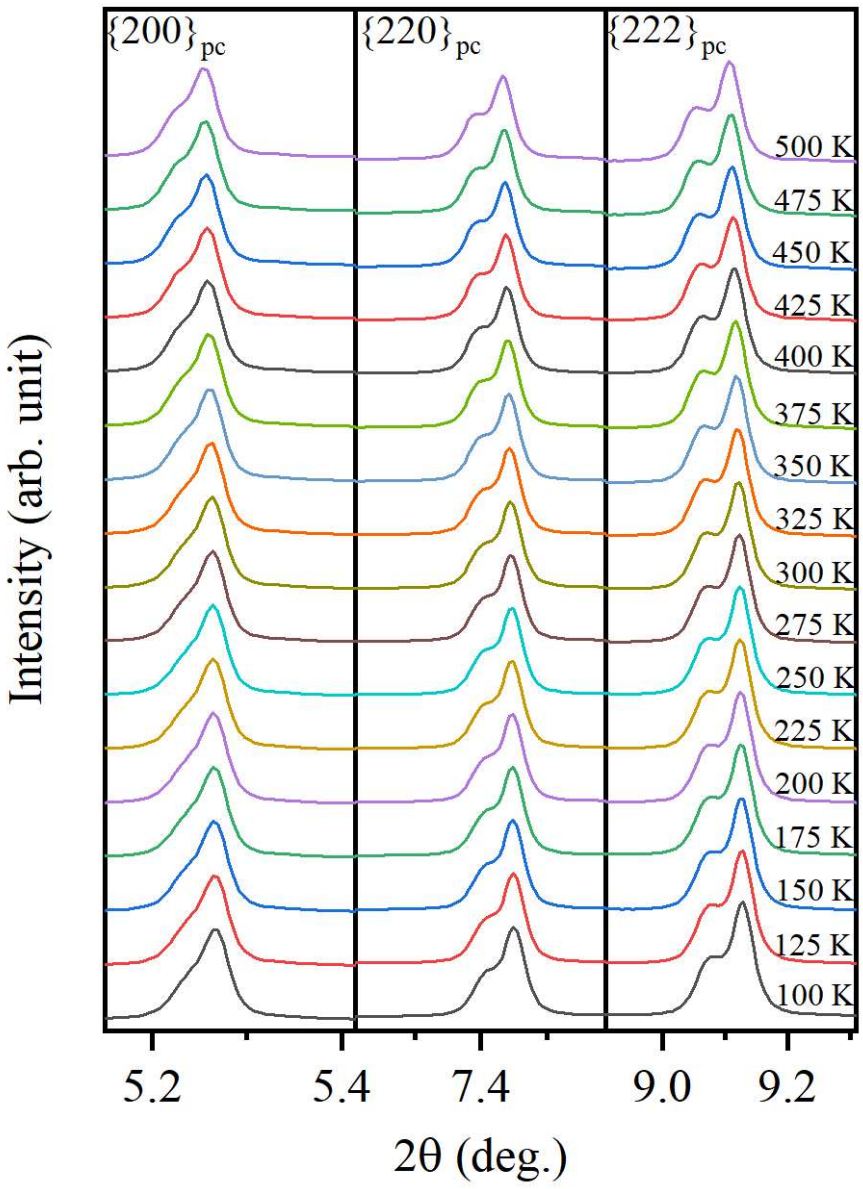

Fig. 6.2 Temperature-dependent evolution of main perovskite reflections *viz.*, $\{200\}_{pc}$, $\{220\}_{pc}$, and $\{222\}_{pc}$ of NN-60BCT.

phases corresponding to Barium Titanate and Sodium Niobate (C_{BT}+C_{NN}). This model fits all the diffraction patterns very well (R_{wp} < 5 %). Figure 6.3 depicts the Le Bail fits of the diffraction patterns at some representative temperatures. Figure 6.4 depicts the unit cell volume of the two cubic phases as a function of temperature. At high temperatures (above the Burns temperature T_B), the unit cell volumes of the two cubic phases exhibit a linear behaviour. However, a noticeable deviation from the linear behavior is observed below T_B. In order to characterise the temperature dependence of the unit cell volume, we have used the Debye-Grüneisen (DG) equation to fit the volume data at high temperatures (above T_B) and extrapolated the DG curve at low temperatures [330]. Interestingly, the fitting confirmed the deviation of the experimental volume from the theoretical(nominal) volume below the Burns temperature ($T_B \approx 400$ K). The departure of experimental volume from the theoretical volume below T_B can be linked with the nucleation and growth of polar nano regions (PNRs). Further, to assess the nature of thermal expansion, we have calculated the volumetric coefficient of thermal expansion (α_V) using the following equation

$$\alpha_V = \frac{1}{V}\frac{\partial V}{\partial T} \tag{6.3}$$

where V is the volume at temperature T and α_V represents the coefficient of thermal expansion (CTE). For a cubic material, the coefficient of linear thermal expansion (α_l) and volume thermal expansion (α_V) follows the relation α_l = (1/3) α_V [330]. The values of α_l for both the cubic phases are of the order of 10^{-6} / K, which is comparable to those observed in similar compounds [270, 330]. To understand the volume gain below T_B, we have used the concept of spontaneous volume ferroelectrostriction (SVFS), which provides a direct correlation between the ferroelectricity and thermal expansion in materials [330, 354]. SVFS is defined as

$$w_s = \frac{(V_{exp} - V_{nm})}{V_{nm}} \times 100\% \tag{6.4}$$

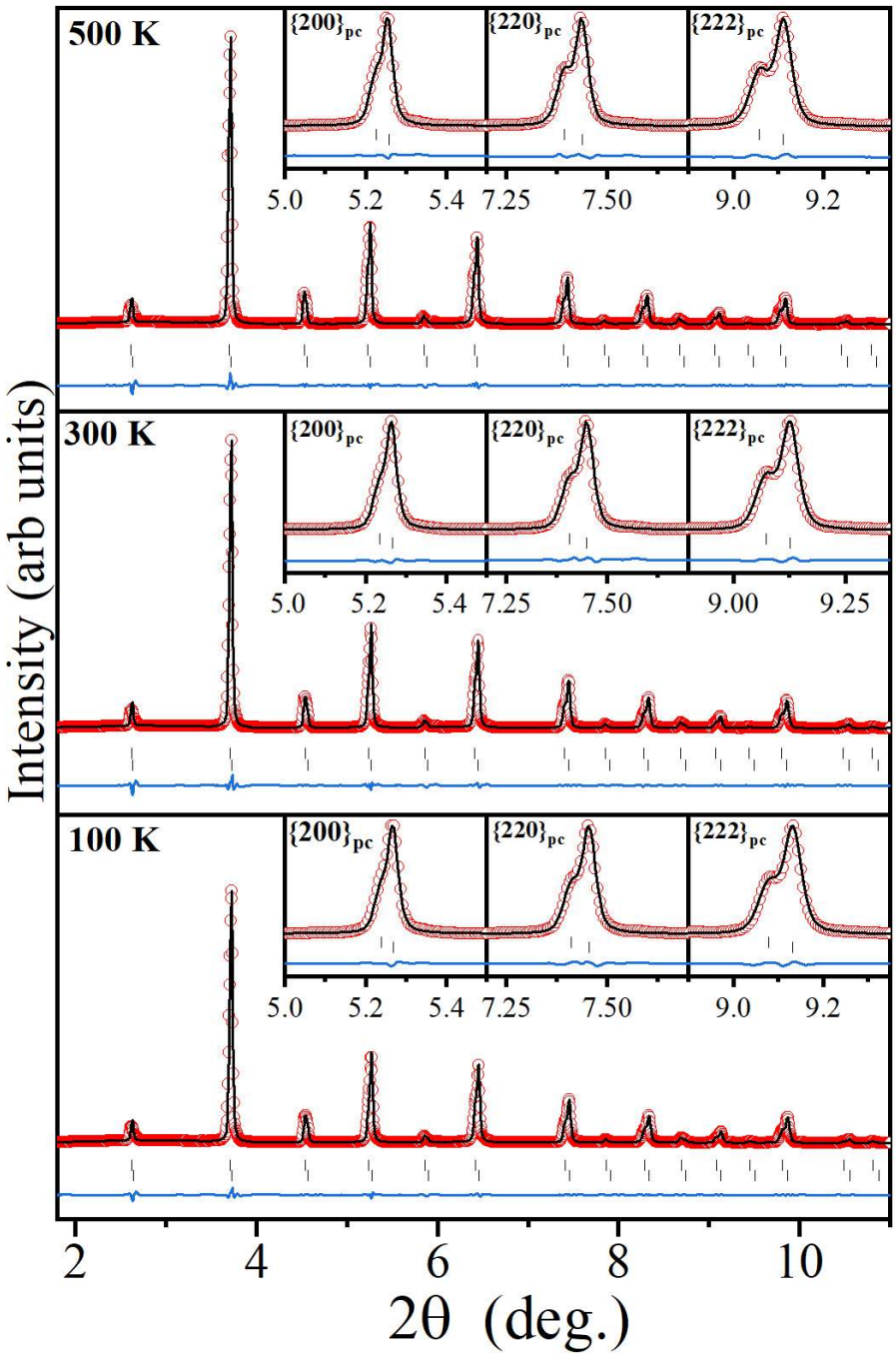

Fig. 6.3 Le-Bail refined diffraction patterns of NN-60BCT at some representative compositions. The inset shows the fitting for $\{200\}_{pc}$, $\{220\}_{pc}$, and $\{222\}_{pc}$ main perovskite reflections.

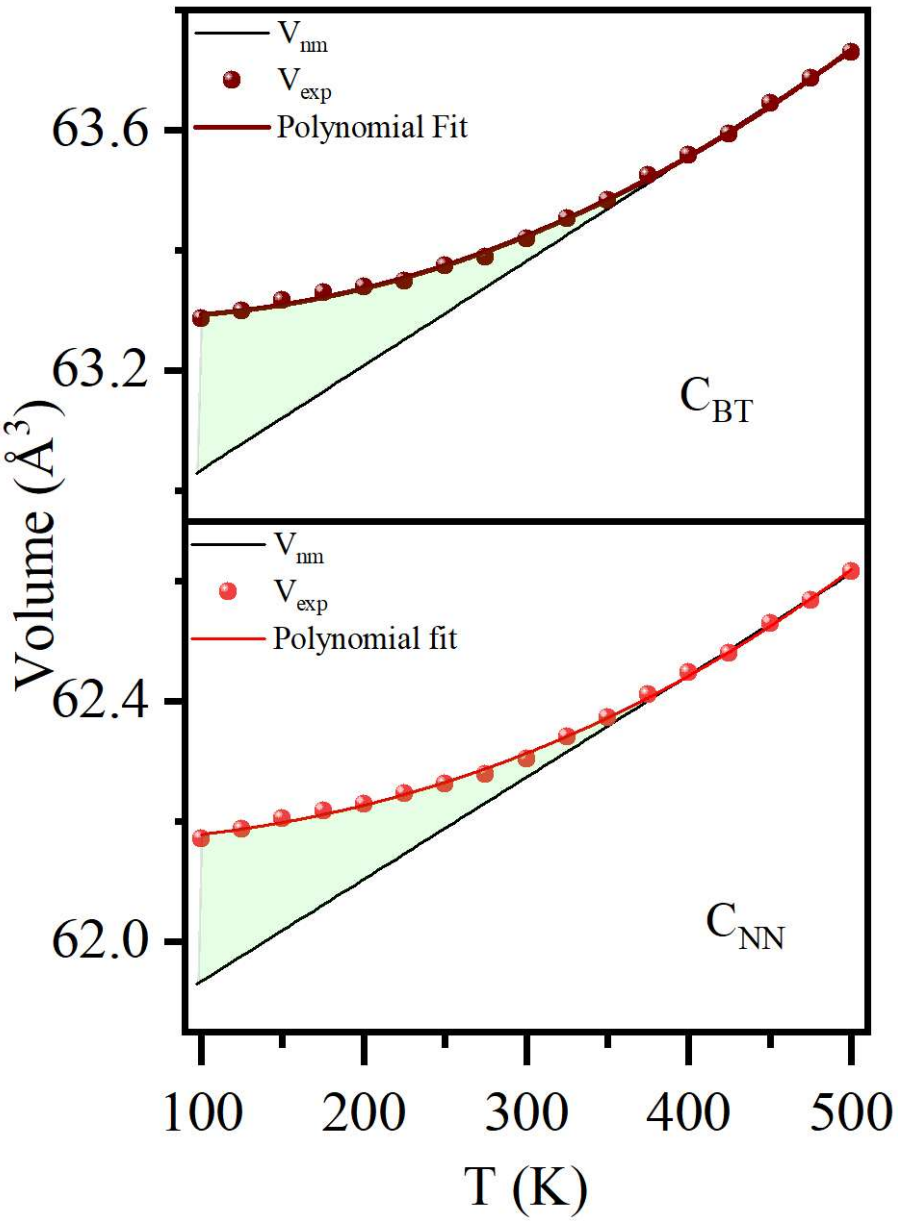

Fig. 6.4 Temperature-dependent variation of volume for the two cubic components present in NN-60BCT ceramic, where the symbol represents the experimental volume, the solid curve represents the polynomial fit of the experimental volume, and the black line represents the nominal volume obtained from the fitting of the Debye-Grüneisen equation for 100-500 K

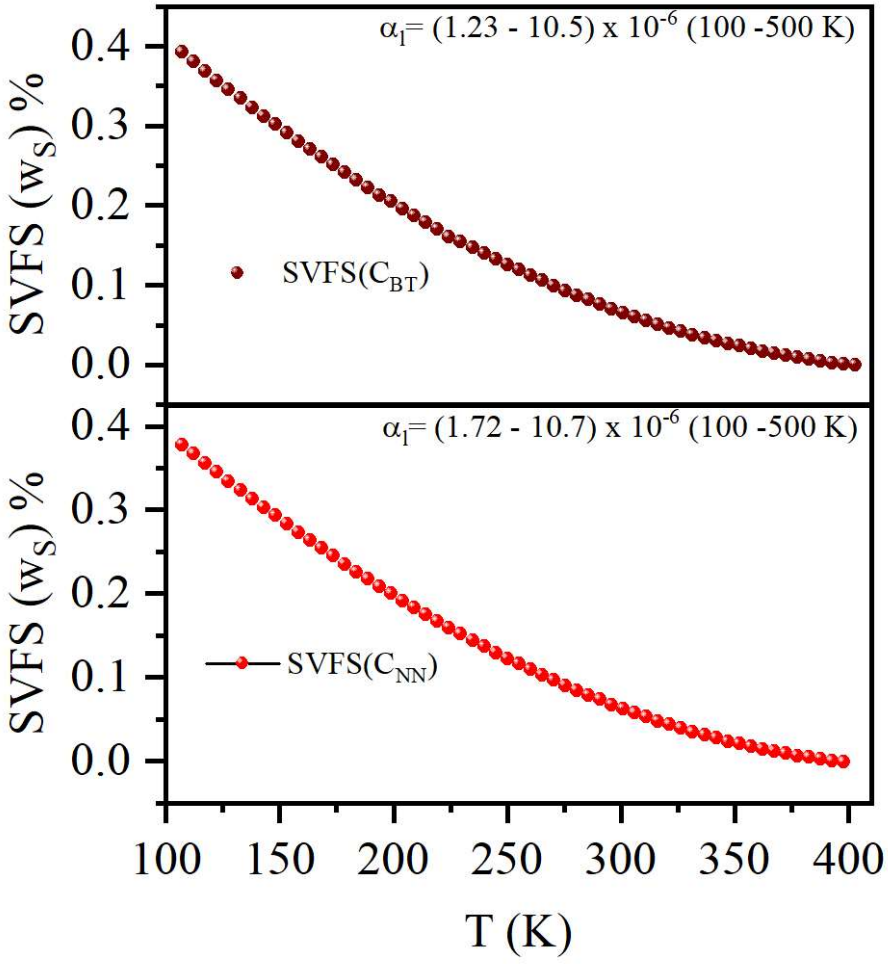

Fig. 6.5 Temperature-dependent variation of spontaneous volume ferroelectrostriction (SVFS) calculated for the two cubic components.

Here, V_{exp} and V_{nm} are the experimental and nominal volumes of the unit cell [330, 354]. Figure 6.5 shows the evolution of SVFS as a function of temperature. It is clearly evident from the figure 6.5 that the SVFS increases ($w_s \approx 0.4\%$ at 100 K for both phases) with the decrease in temperature.

Anomalous thermal expansion (ATE) observed in normal ferroelectrics and relaxor ferroelectrics primarily originates from the enhancement of polar/ferroelectric ordering at long and/or short ranges [330], and can be quantified by volume gain at low temperatures. The volume gain observed in normal/relaxor ferroelectrics is referred to as ferroelectrostriction (ferroelectrovolume effect) [330]. In normal ferroelectrics, the **long-range polar ordering** (spontaneous polarization) appears below the Curie temperature (T_C) and is accompanied by spontaneous strain (ferroelectrostriction) in the crystalline lattice. As a result, the material contracts on cooling and shows a volume gain. On the other hand, in relaxor ferroelectrics, anomalous thermal expansion arises from the progressive correlation and freezing of polar nano-regions at low temperatures, which results in localized strains, thereby reducing the unit cell volume [270, 301, 330]. Therefore, the behaviour of thermal expansion in relaxors results from the coupling of *local polar distortions* with the crystalline lattice. Now, in order to investigate the short-range structural ordering (PNRs) in the system, we have employed two different techniques, *viz.,* Raman spectroscopy and Pair Distribution Function (PDF). These techniques help us in analyzing the short-range atomic ordering existing in the crystalline materials.

6.3.3 Raman Analysis

Raman analysis is an essential tool for investigating the local-polar distortion in relaxor ferroelectrics [262, 317]. As discussed in chapter 3, NN-60BCT shows evidence for rhombohedral-like short-range polar ordering at ambient conditions, characterised by the presence of ferroelectric modes in the room temperature Raman spectra. In this chapter, we

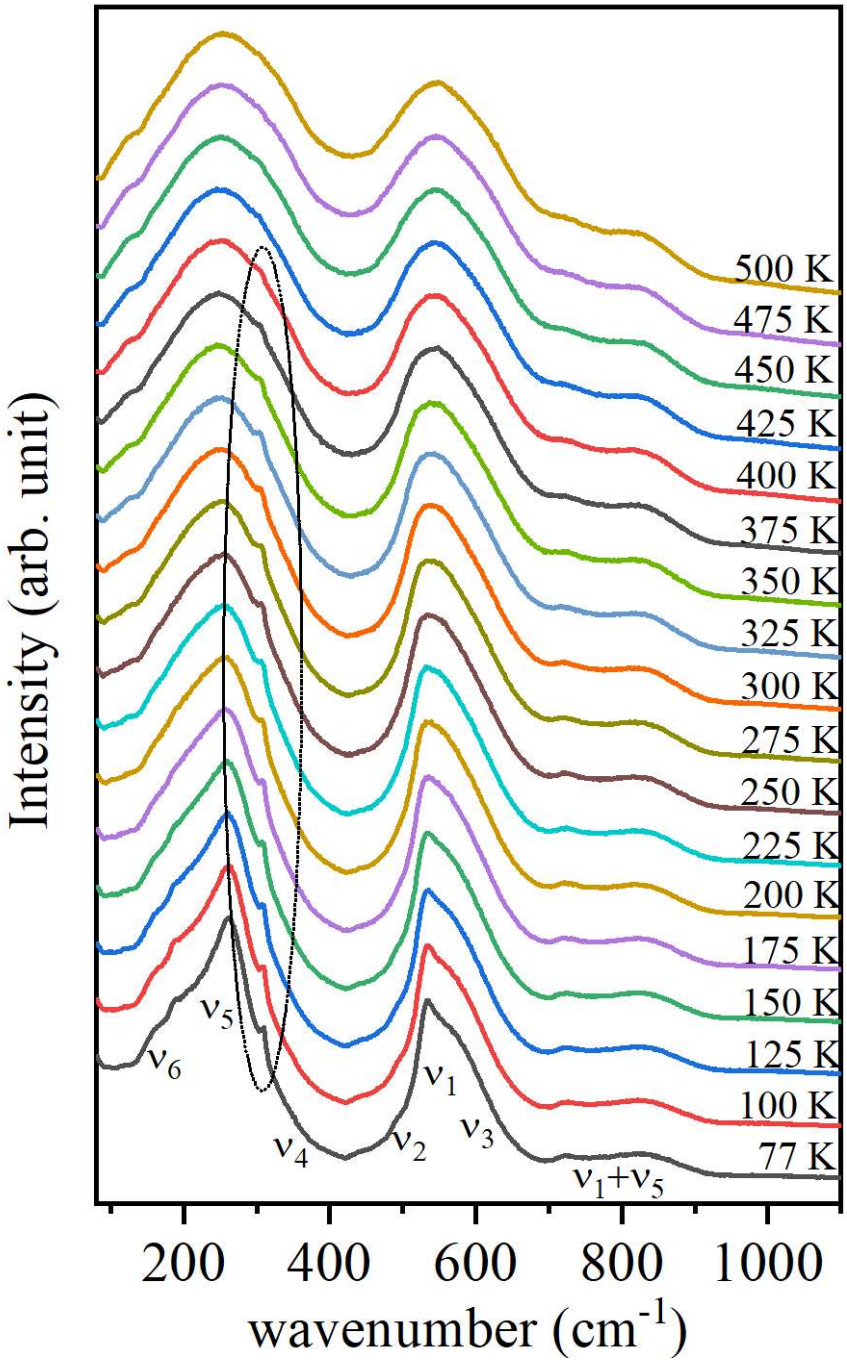

Fig. 6.6 Temperature-dependent Raman spectroscopy data for NN-60BCT.

extended our Raman studies for NN-60BCT by performing temperature-dependent Raman analysis in a wide temperature range, 77-500 K (see figure 6.6). All the Raman spectra were corrected for the Bose-Einstein factor. Although the long-range order within the studied temperature range ($100 \leq T \leq 500$ K) is centrosymmetric with $Pm\bar{3}m$ space group, yet Raman spectra show significant scattering, suggesting the presence of noncentrosymmetric polar nano regions (PNRs). The room temperature Raman spectrum of NN-60BCT is similar to what has been reported earlier [71].

As discussed in previous chapters, the Raman spectra of perovskites can be classified into three different regions: (i) translational modes of A-site cations, (ii) bending modes of O-B-O bonds, and (iii) stretching modes of B-O bonds [33, 286]. In relaxor ferroelectrics, the interpretation of Raman spectra becomes challenging because the selection rules are relaxed due to factors such as atomic site disorder, off-centre displacements, **chemical ordering**, and local symmetry breaking [120, 153]. As a result, assigning individual vibrational modes corresponding to long and short-range orders becomes tricky. Additionally, due to the disordered nature of the material (resulting from multiple cations occupying the same crystallographic site), the number of observed Raman modes is often different from the theoretical prediction. Therefore, it is common practice to refer the **broad features (arsing due to overlapping modes)** in the spectra as Raman bands. In line with previous studies on perovskite-based ferroelectrics, we have designated these bands as ν_1 to ν_6. Here, the bands ν_1, ν_2, and ν_3 are associated with the stretching vibrations of B–O bonds, while ν_4, ν_5, and ν_6 correspond to bending vibrations of O-B-O bonds (see Figure 2.6). Figure 6.6 shows that the Raman bands become sharper at low temperatures, suggesting an enhancement in structural ordering. We have deconvoluted the Raman spectra using suitable Lorentzian peaks. Following the literature on similar materials, the Raman mode observed around 305 cm^{-1} can be considered as a distinct feature of short-range polar ordering [223, 261]. Therefore, we have selected this mode to track the evolution of short-

range polar symmetry. Figure 6.7 illustrates the evolution of the relative intensity of the Raman mode corresponding to the wavenumber ≈ 305 cm^{-1} (obtained after deconvolution). Here, we can see that the intensity of the Raman mode increases with a decrease in

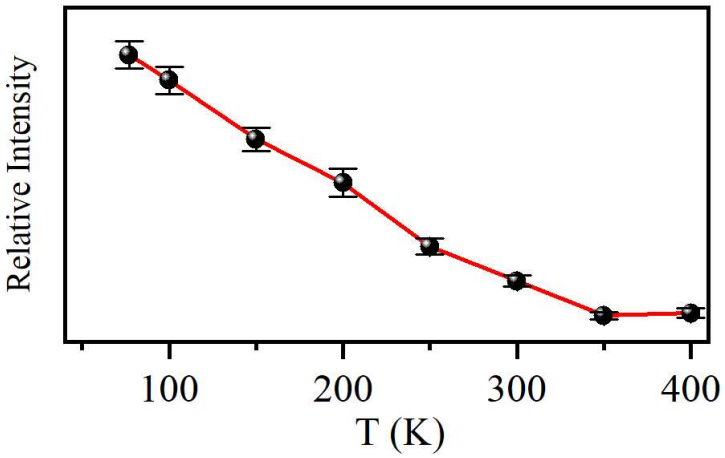

Fig. 6.7 Temperature-dependent evolution of deconvoluted relative intensity of the Raman mode present around ≈ 305 cm^{-1}.

temperature, providing evidence for the enhancements in intra/inter polar correlations at low temperatures. The unusual thermal expansion observed in NN-60BCT at low temperatures has been attributed to an enhancement in interactions/correlations among PNRs(short-range ordering). In the next section, we will identify the symmetry at short ranges using Pair Distribution Function (PDF) analysis.

6.3.4 Pair Distribution Function Analysis

The pair distribution function (PDF) method is an important tool in characterising complex local structures in perovskite-based relaxor ferroelectrics [165, 222, 287, 288]. Generally, the short-range structural distortions in relaxor ferroelectrics have been quantified by refining the atomic PDFs. Figure 6.8 (a) shows the temperature-dependent X-ray PDFs of NN-60BCT in the spatial range $1.7 \leq r \leq 6$ Å. We have marked the correlation peaks corresponding to B-O, A-O/O-O, and A-A/B-B/O-O bonds. The broad nature of PDF

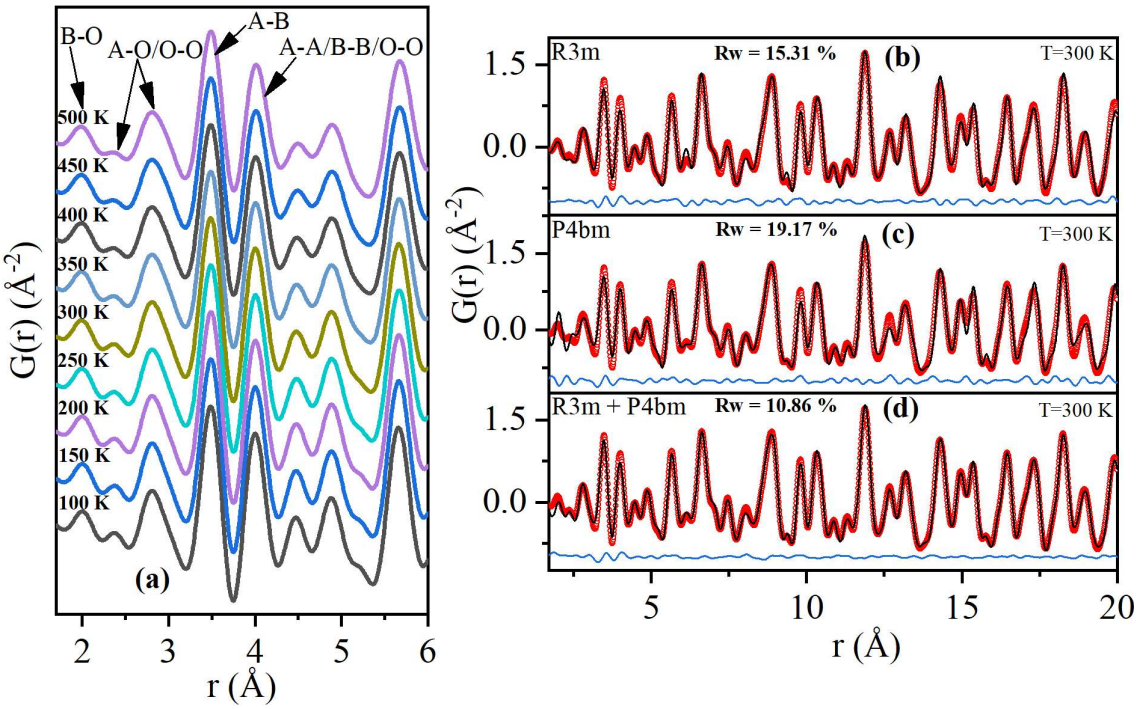

Fig. 6.8 (a)Temperature-dependent evolution of experimental atomic PDFs of NN-60BCT. Correlation peaks arising from different bonds are marked using arrows. Fitting of the PDF profiles at 300 K using (b) *R3m*, (c) *P4bm*, and (d) *R3m+P4bm* models along with their goodness of fit parameters.

peaks can be attributed to the presence of multiple cations at equivalent crystallographic sites. Moreover, the PDF peaks further broaden on increasing temperature, suggestive of an increase in structural disorder due to an enhancement in thermal energy. For quantitative analysis of the short-range structural distortion as a function of temperature, we have performed fitting of G(r) using the PDFgui program [225]. To investigate the local symmetry of NN-60BCT at room temperature, we refined the atomic pair distribution function (PDF) using a rhombohedral phase (space group: *R*3*m*) speculated from Raman spectroscopy analysis [71]. However, this model did not give a satisfactory fit to the experimental PDF. In addition, large thermal parameters indicate the inadequacy of the model to fit the PDF pattern. Subsequently, we explored the tetragonal *P*4*bm* phase, which is the local symmetry of NN-25BCT concluded in Chapter 5. Similar to the rhombohedral phase, the tetragonal phase failed to provide a satisfactory fit. Next, we employed a

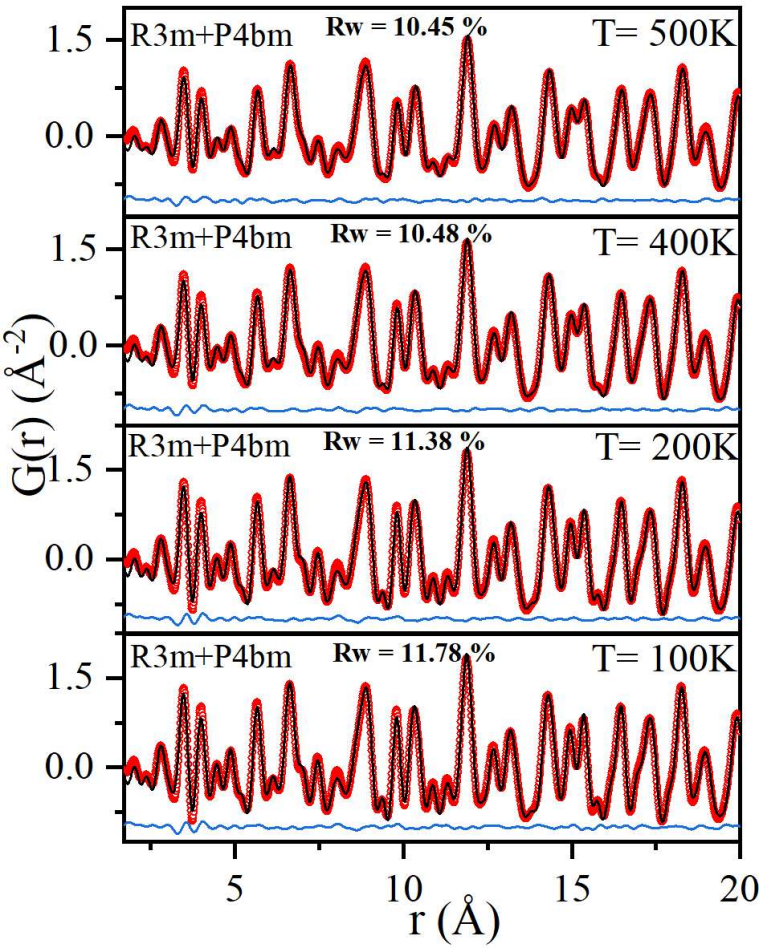

Fig. 6.9 PDF fitting of NN-60BCT using the two-phase (*R3m+P4bm*) model shown at some representative temperatures along with goodness of fit parameters.

two-phase $R3m + P4bm$ model. This two-phase model resulted in a significantly improved fit to the PDF, with reasonable goodness-of-fit values (see Fig. 6.8 (b)- (d)). These findings suggest the coexistence of two types of short-range polar order in a non-polar matrix, corresponding to two distinct types of polar nanoregions (PNRs):

- Rhombohedral PNRs (with *R3m* space group) originating from the end member $Ba_{0.9}Ca_{0.1}TiO_3$ (BCT), and
- Tetragonal PNRs (with *P4bm* space group) originating from the end member $NaNbO_3$ (NN)

Furthermore, $R3m + P4bm$ model provides the best fit at all the studied temperatures (see Fig. 6.9), confirming the stability of the two phases at short ranges for NN-60BCT in a wide temperature range (100 $\leq$ T $\leq$ 500 K).

Figure 6.10 provides a schematic representation of the evolution of polar nano regions (PNRs) as a function of temperature. At very high temperatures (T >>> T_B), the structure of NN-60BCT exhibits two long-range cubic structures C_{BT} and C_{NN} corresponding to the two parents of the solid solutions, *viz.,* $NaNbO_3$ (elementary cell with smaller volume) & $Ba_{0.9}Ca_{0.1}TiO_3$ (elementary cell with larger volume). On decreasing temperatures below T_B, two types of PNRs originating from rhombohedral of BT-like and tetragonal of NN-25BCT-like start growing (see Fig. 6.10). The correlation among these PNRs enhances at low temperatures due to a decrease in thermal disorder. Therefore, the ordering of PNRs in the disordered non-polar matrix develops strain, resulting in anomalous thermal expansion observed at long ranges [355].

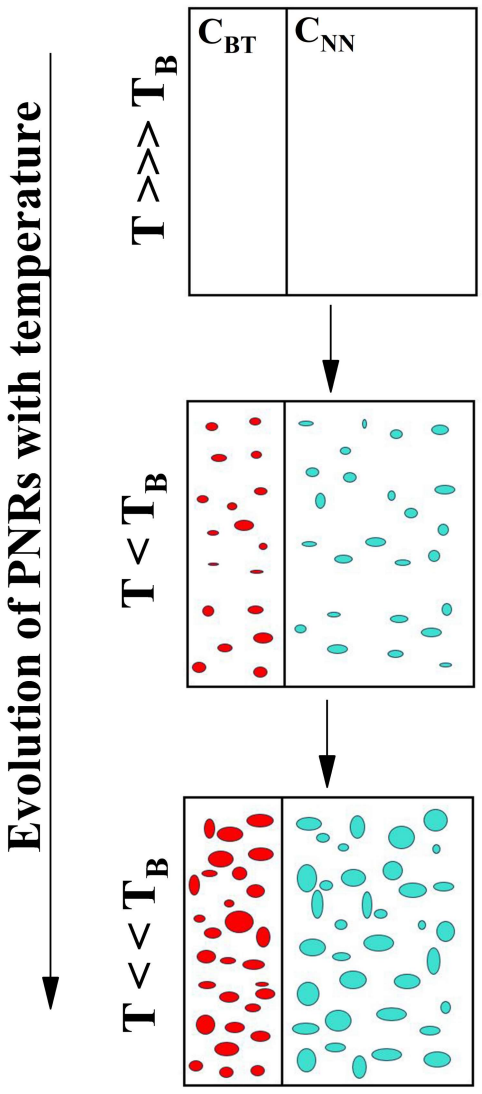

Fig. 6.10 Evolution of PNRs in NN-60BCT as a function of temperature. The red and turquoise blue are the rhombohedral and tetragonal PNRs, embedded in BT-like (C_{BT}) and NN-like (C_{NN}) in cubic matrices, respectively.

6.4 Conclusion

In summary, we conducted temperature-dependent structural investigations on a lead-free Sodium Niobate-based relaxor (NN-60BCT). Dielectric analysis suggests relaxor-like behaviour of the present system, having Burns temperature (T_B) and Vogel-Fulcher (T_{VF}) freezing temperature at $\approx$ 400 K and $\approx$ 170 K, respectively. Further, temperature-dependent SXRD measurement confirms the absence of a long-range phase transition below T_{VF}, suggesting canonical relaxor-like behaviour. Interestingly, the unit cell volume of both components shows anomalous thermal expansion below the Burns temperature. This anomalous thermal expansion has been attributed to the progressive interaction originating from the nucleation and growth of polar nano-regions (PNRs), thereby resulting in ferroelectrostriction. Raman spectroscopy measurements reveal an enhancement of the Polar phased regions, which are evident from the increase in intensity (on decreasing temperature) of the ferroelectric Raman mode present around $\approx$ 305 cm^{-1}. Further, we performed Pair Distribution Function (PDF) analysis to quantify the short-range structural distortions in NN-60BCT. This analysis helped us in identifying the symmetry of the PNRs, revealing the presence of two different local symmetries : (i) Rhombohedral(space group: *R3m*) (ii)Tetragonal (space group: *P4bm*). Unlike conventional relaxors, which typically exhibit a single type of polar nano-region (PNR), this system displays the formation of two distinct types of nano-polar clusters. As the temperature decreases, these polar clusters grow and correlate more strongly with each other. This enhanced correlation leads to a phenomenon known as ferroelectrostriction (ferroelectrovolume effect), where the material contracts or expands due to the ordering of electric dipoles. The ability to control the expansion and contraction of this material makes NN-60BCT a promising candidate for applications in devices requiring controlled thermal expansion.